Myocardial perfusion SPECT using a rotating multi-segment slant-hole collimator

Chi Liu[a)]
Department of Radiology and Radiological Sciences, School of Medicine, Johns Hopkins University, Baltimore, Maryland 21287 and Department of Environmental Heath Sciences, Bloomberg School of Public Health, Johns Hopkins University, Baltimore, Maryland 21287

Jingyan Xu and Benjamin M. W. Tsui
Department of Radiology and Radiological Sciences, School of Medicine, Johns Hopkins University, Baltimore, Maryland 21287

(Received 11 August 2009; revised 15 January 2010; accepted for publication 19 January 2010; published 17 March 2010)

Purpose: A rotating multi-segment slant-hole (RMSSH) collimator is able to provide much higher (~3 times for four-segment collimator with 30° slant angle) sensitivity than a parallel-hole (PH) collimator with the similar spatial resolution for imaging small organs such as the heart and the breast. In this article, the authors evaluated the performance of myocardial perfusion SPECT (MPS) using a RMSSH collimator compared to MPS using the low-energy high-resolution parallel-hole collimators.
Methods: The authors conducted computer simulation studies using the NURBS-based cardiac-torso phantom, receiver operative characteristic (ROC) analysis using the channelized Hotelling observer, physical phantom experiments, and pilot patient studies to evaluate the performance of MPS using a rotating four-segment slant-hole (R4SSH) collimator with respect to MPS using a PH collimator.
Results: In the simulation study, the R4SSH MPS provides images with superior contrast-noise trade-off than those of PH MPS with the same acquisition time. The defect detectability in terms of the largest area under the ROC curve for R4SSH MPS is significantly higher than those of PH MPS with p-values <0.01. In the phantom experiments, the R4SSH MPS images with 7.5 min acquisition had similar noise level and overall image quality as those of PH MPS with 21 min acquisition. Pilot patient studies showed that with the same acquisition time, the R4SSH SPECT using a single-head camera gave images with similar quality as those of PH SPECT using a dual-head camera.
Conclusions: The RMSSH SPECT has a potential to improve the coronary artery disease detection and workflow of SPECT imaging acquisition due to the high sensitivity property of the RMSSH collimator.
[DOI: 10.1118/1.3310386]

Key words: myocardial perfusion SPECT, rotating multisegment slant-hole collimator, parallel-hole collimator

I. INTRODUCTION

Coronary artery disease (CAD) is the leading cause of death in most industrialized countries. Single photon emission computed tomography (SPECT) has become an important diagnostic method of the clinical management of this disease. The conventional myocardial perfusion SPECT (MPS) uses parallel-hole (PH) collimators. To improve the MPS imaging, rotating slant-hole collimators had been proposed as an alternative to parallel-hole collimators by several groups.[1–6] We have focused on developing a rotating multi-segment slant-hole (RMSSH) collimator with multiple segments; as shown in Fig. 1(a), each segment has parallel-hole collimators that slant toward a common-volume-of-view (CVOV) where the object is to be imaged. Each segment provides a projection image of the object at a different viewing angle. The collimator is able to rotate around its central axis in order to obtain multiple projection views.

The geometrical efficiency of a collimator is inversely proportional to the square of collimator length. With the same collimator thickness of a parallel-hole collimator, the length of a slant-hole collimator is elongated by a factor of $1/\cos\sigma$, where σ is the slant angle shown in Fig. 1(a).[6] Therefore, a RMSSH collimator has $N\cos^2\sigma$ times the sensitivity as that of a parallel-hole collimator with the same thickness and hole size, where N is the number of segments. With the same hole size of a parallel-hole collimator, the hole aperture on the front face of a slant-hole collimator would be elongated in the direction of slant but remains the same in the direction perpendicular to the slant direction. Thus, compared to a parallel-hole collimator with the same thickness and hole size, the collimator resolution of a slant-hole collimator is degraded by a factor of $1/\cos\sigma$ in the direction of hole slant and maintains equal in the direction perpendicular to the slant direction, leading to a slightly

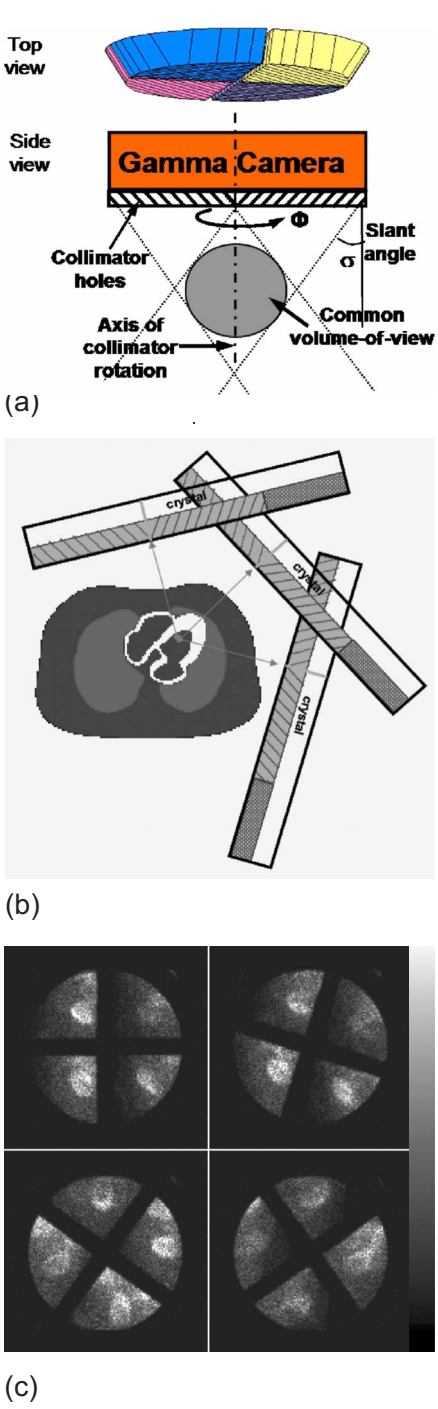

FIG. 1. (a) Cross-sectional view through the center of a R4SSH collimator. (b) Configuration of acquisition geometry with three camera positions for RMSSH myocardial SPECT. (c) Sample projections of a R4SSH cardiac SPECT patient study.

worse overall resolution averaged over the two directions.[6] For example, a rotating four-segment slant-hole (R4SSH) collimator with a slant angle of 30° provides three times the sensitivity with ~8% increase in the averaged resolution compared to a parallel-hole collimator with the same thickness and hole size.[6] Therefore, for the same acquisition time, the RMSSH SPECT can provide images with substantially lower noise than PH SPECT with similar collimator resolution; or using much shorter acquisition time or less patient dose, the RMSSH SPECT can give images with similar noise level as that of the PH SPECT with similar collimator resolution but much longer acquisition time or larger patient dose.

Due to the special geometry, a RMSSH collimator has a smaller field-of-view (FOV) than that of a parallel-hole collimator. For example, a four-segment slant-hole collimator with a slant angle of 30° and a collimator diameter of 40 cm provides a common-volume-of-view [the shaded sphere in Fig. 1(a)] with a diameter close to 12 cm. Thus, the RMSSH collimator trades the FOV size for additional sensitivity and is beneficial for imaging small organs like the heart.

In order to perform MPS study using the RMSSH collimator, as shown in Fig. 1(b), the gamma camera needs to be placed at several (usually three or four) positions around the patient's body. At each camera position, the collimator rotates at several (usually 12–15) stops to obtain enough projection data for image reconstruction with reasonable sampling and image resolution. Figure 1(c) shows sample projection images of different rotation stops of a patient study. In this paper, we used three camera positions for a R4SSH collimator with a slant angle of 32.5° and 12 or 15 rotation stops for each camera to satisfy the conditions for complete angle reconstruction.[6,7] With only three camera positions, the gamma camera can be placed very close to the patient with a much shorter imaging distance that leads to higher spatial resolution than conventional SPECT with 180° acquisition. In this study, the distance between the collimator face and center of the heart for each camera position is 14.5 cm, which is much smaller than the typical radius of rotation (~25 cm) of conventional SPECT with circular orbit.

Compared to conventional MPS using LEHR collimators with the similar spatial resolution, the RMSSH myocardial SPECT is expected to have advantages in both image quality and patient management. First, due to the high sensitivity property described above, the R4SSH SPECT can provide images with substantially lower noise for the same dose and acquisition time than those of the PH SPECT. Second, the patients in the conventional MPS procedure are usually asked to raise both arms up and it would be potentially more comfortable if only one arm is up during the scan. The imaging geometry of R4SSH SPECT requires a patient to lift up only his/her left arm, allowing the patient to be imaged in a more comfortable position to reduce the chance of body motion. We have developed the RMSSH technique and performed feasibility studies primarily in the context of breast and cardiac imaging with preliminary phantom evaluations.[6] In this study, we conducted computer simulations, channelized Hotelling observer (CHO) and receiver operative characteristic (ROC) analysis, physical phantom experiments, and pilot patient studies to thoroughly evaluate the performance of RMSSH SPECT with respect to conventional SPECT with parallel-hole collimators in clinical myocardial perfusion imaging.

TABLE I. Collimator parameters of the R4SSH and GE LEHR collimator used in simulation.

	R4SSH	GE LEHR
Hole size (cm)	0.19	0.15
Hole length (cm)	5.93	3.5
Slant angle (deg)	32.5	···
Collimator thickness (cm)	5.00	3.5
Distance from the collimator face to the CVOV center (cm)	14.45	···
Diameter of the CVOV (cm)	11.87	···
Average collimator resolution at 14.45 cm (cm)	0.81	0.77
Sensitivity ($\times 10^{-3}$)	0.17	0.07

II. MATERIALS AND METHODS

II.A. Computer simulation studies

II.A.1. Phantom and simulations

We used the 3D NURBS-based cardiac-torso (NCAT) phantom[8] with realistic Tc-99m radioactivity distribution to simulate SPECT projection data. A perfusion defect at the lateral location in the short-axis view with a contrast of 50% less than the normal myocardium was created. The defect had a size of 60° radial range and 1 cm axial length. The organ activity ratios were 75, 35, and 2 for the heart, liver, and the background, respectively.

The PH collimator in this study had the same parameters of the General Electric (GE) LEHR collimator (Haifa, Israel). The R4SSH collimator we simulated is the one we designed and was fabricated by Nuclear Fields USA (Des Plaines, IL). The parameters of both collimators are shown in Table I. To simulate the R4SSH SPECT projections, we used three camera positions with 60° interval and 12 collimator rotation stops over 90° at each camera position. The three camera positions were −10°, 50°, and 110°, respectively, from lateral to anterior. For PH SPECT, the projection data were acquired by using the regular clinical protocol, 64 views over a 180° arc, from LPO 45° to RAO 45°, with a radius-of-rotation (ROR) of 22.5 cm. Both PH and R4SSH SPECT data were simulated with analytical projectors,[9] including the effect of attenuation and collimator-detector response to generate the noise-free projections, which were scaled to the clinical counts level at ~15 min acquisition; Poisson noise was then added to form noisy projections.

II.A.2. Reconstruction and evaluation

The ordered-subset expectation-maximization (OS-EM) algorithm with four subsets was used to reconstruct both the PH and R4SSH projections.[10] For each subset of R4SSH data, the number of projections was nine and all projections were balanced. The special geometry of R4SSH SPECT was incorporated into the OS-EM reconstruction through a rotating-shearing projector-backprojector.[9] Attenuation compensation (AC) was implemented by using the NCAT generated attenuation map. The reconstructed images had a matrix size of $128\times128\times128$ and voxel size of 0.31 cm. No postfilter was applied to the reconstructed noisy images.

Image quality was evaluated in terms of defect contrast and noise level. From the noise-free images, we measured the average pixel value of defect as A_{defect} and average pixel value in the normal myocardium as A_{normal}. The defect contrast was then defined as

$$\text{Contrast} = \frac{A_{\text{normal}} - A_{\text{defect}}}{A_{\text{normal}} + A_{\text{defect}}}. \quad (1)$$

In the noisy images, the noise level was measured by calculating the average normalized standard deviation (NSD) of the voxels in specified uniform ROIs within the myocardium. The NSD of each voxel i in the image was first calculated by dividing the voxel standard deviation (SD) by the voxel mean as follows:

$$\text{NSD}_i = \frac{\text{SD}_i}{\text{Mean}_i} = \frac{\sqrt{1/N-1\Sigma_{n=1}^{N}(x_{i,n}-\mu_i)^2}}{\mu_i}, \quad (2)$$

where $x_{i,n}$ is the value at voxel i for noise realization n, μ_i is the ensemble mean value of voxel i, and N is the number of noise realizations. Then the NSD was averaged over all voxels in the ROI to obtain the averaged NSD. In this study, 30 realizations of noisy data were used to calculate the voxel standard deviation and mean. The ROI was chosen as a relatively uniform 3D volume within the normal myocardium with a total number of 42 voxels.

II.B. Channelized Hotelling observer study

II.B.1. Simulation and reconstruction

Since the evaluation metrics of contrast and noise is an estimation of physical parameters and may not match human observer performance in a detection task, we evaluated the performance of R4SSH MPS with respect to the traditional PH MPS in terms of defect detection using the ROC analysis and CHO.[11,12]

The task was to detect cardiac perfusion defects located at the lateral and anterior locations in the short-axis view. The defects had a size of 60° radial range and 1 cm axial length. Unlike the defects with 50% contrast generated in Sec. II A 1, the defect in the ROC study had 15% lower activity than the normal myocardium. We chose this 15% contrast by doing a small size pilot CHO study so that the AUC values would be neither too high (larger than 0.95) nor too low (smaller than 0.55).

The projection simulations are similar with those in Sec. II A 1 with the same collimator parameters and acquisition time. Both PH and R4SSH SPECT images were reconstructed using the OS-EM algorithm with four subsets without and with AC. The reconstructed images were postfiltered by the Butterworth filter with different cutoff frequencies. The number of iterations for OS-EM and the cutoff frequency for the Butterworth poster filter were optimized using CHO in terms of the highest AUC values. The final reconstructed images were resliced to short-axis view and extracted to two-dimensional 32×32 images centered on the defect. The pixel values in the extracted images were windowed to integer values in the range of 0–255 so that the

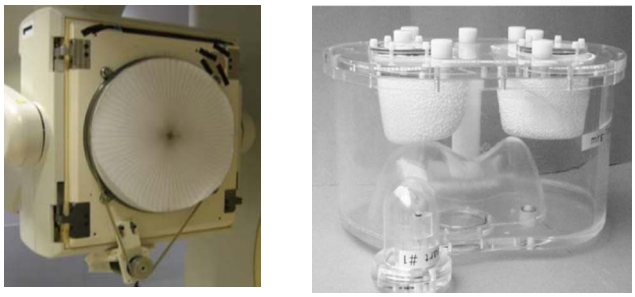

(a) (b)

FIG. 2. (a) The R4SSH collimator with rotating motor mounted on the Philips Precedence® SPECT/CT system. (b) The data spectrum's anthropomorphic torso phantom with heart insert.

maximum value in the heart was mapped to 255 and negative values generated by postfiltering were truncated to zero.

II.B.2. Application of the CHO

To apply the CHO, four band-pass channels in the frequency domain were used to model human visual response.[13,14] These channel sets have been used in several cardiac studies and shown good correlation with human observer performance.[13–16] The spatial domain templates were obtained by taking the inverse Fourier transform of the four channels in frequency domain and shifting the template centers to the defect centroid. For each reconstructed and resliced image, a four-element feature vector was obtained by taking the dot product of the extracted image and the spatial domain templates for each channel.

To generate each ROC curve, we used 96 images for training and 96 images for testing. The defect-present images are constructed in this way: Two defect locations $\times$ six noise realizations $\times$ eight uptake ratios variations $=96$ images. For defect-absent images, we generated 12 noise realizations rather than six to make the total images for normal and abnormal the same so that the variances for true positive fraction and false positive fraction of each point on the ROC curve are the same.[17] Note that there are six (12 for defect-absent) noise realizations. CHO was trained using the images from the first three (six for defect-absent) noise realizations, and tested using the images from the remaining three (six for defect-absent) noise realizations, so that the training and testing images have similar statistical properties.

II.B.3. ROC analysis

The ROC analysis followed the strategies in Refs. 17–19. The decision variables obtained from CHO were imported into the LABROC4 program developed at University of Chicago to get the mean and standard deviation of AUC values.[18,20,21] For each imaging method, the combination of iteration number and cutoff frequency giving the highest AUC value was considered the one offering the best performance. There were four imaging methods being compared: R4SSH SPECT without and with AC and PH SPECT without and with AC. The highest AUC values given by each method were compared using CLABROC program developed at University of Chicago to test if the differences were significant.

II.C. Physical phantom study

The R4SSH collimator fabricated by Nuclear Fields was mounted on the Philips Precedence® (Philips Healthcare, San Jose, CA) SPECT/CT system [shown in Fig. 2(a)]. A stepping motor controlled the rotating mechanism. Each time the motor rotates, the controller of the motor sends a transistor-transistor logic (TTL) signal to the electrocardiogram input of the Precedence® system. We acquired one list-mode file for each camera position and rebinned the list-mode file into 15 projections according to the detected TTL signal.

A Data Spectrum® anthropomorphic cardiac-torso phantom including heart, lungs, liver, and spine insets shown in Fig. 2(b) was used to acquire experimental data. A total activity of 555 MBq Tc-99m Sestamibi was injected into the phantom. The activity ratios for heart:liver:background were 10:5:1. There was no activity in the lung.

For R4SSH SPECT, the three camera positions were set at 0°, 60°, and 120° from the lateral to the anterior view. We adjusted each camera position by putting the projections of the heart at the center of each collimator segment to avoid truncation. The collimator rotated for 15 stops at each camera position. For PH SPECT, a single-head detector was used to acquire 64 projections over 180° orbit, from LPO 45° to RAO 45°, with a ROR of 25 cm. The acquisition time of PH SPECT was ~21 min (20 s/view, 64 views). The R4SSH collimator has 2.8 times sensitivity as that of the PH collimator with similar resolutions; therefore we conducted the R4SSH SPECT study with a total acquisition time of ~7.5 min (10 s/view, 45 views), which is about 1/2.8 as that of the PH SPECT. Both R4SSH and PH SPECT projections were reconstructed with OS-EM without any compensation. The R4SSH data were reconstructed with five subsets and PH data were reconstructed with four subsets to keep the integer number of projections in each subset. The matrix size of all reconstruction images was $128\times128\times128$ and voxel size was 0.47 cm

II.D. Pilot patient studies

Five patients were recruited for this study from those scheduled for PH Tc-99m MPS study on the Precedence® system. The study was approved by the Institutional Review Board. Prior consent was obtained from each patient recruited in the study. After the routine rest/stress MPS study for each patient using LEHR collimators and CT scans, the patient would get off the patient bed for a break (usually ~15 min) during the collimator exchange.

In this pilot study, the PH SPECT used a dual-head camera and an acquisition time of 15 min. The R4SSH SPECT data were acquired with ~15 min (19 s/collimator stop, 15 stops, three camera positions) using a single-head camera as we only have one R4SSH collimator at the current stage. Thus, although the R4SSH collimator has 2.8 times sensitivity as than that of the PH collimator, there was only 1.4 times

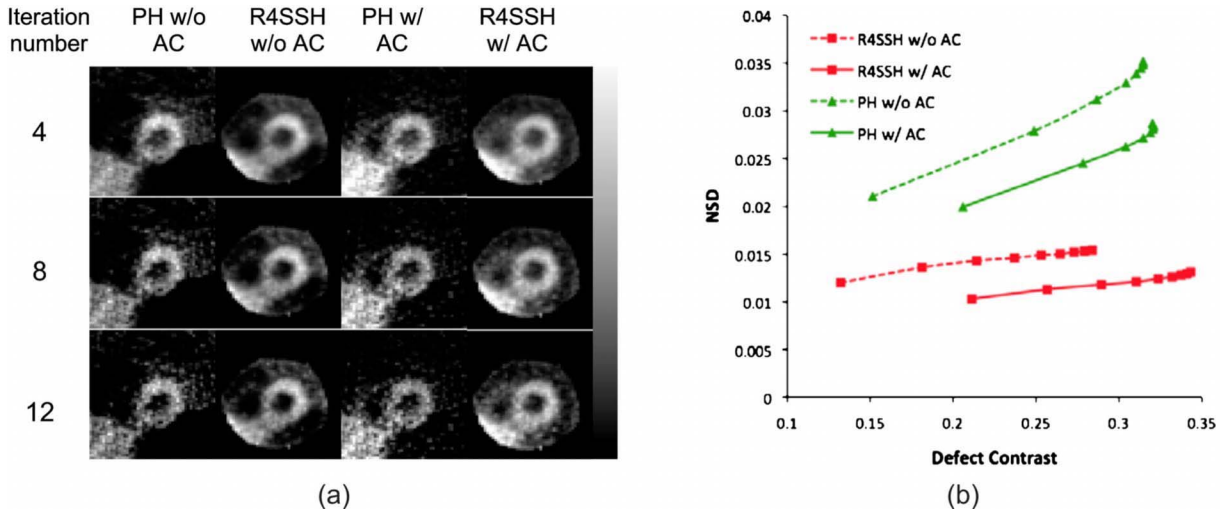

FIG. 3. (a) Sample short-axis slices of PH and R4SSH SPECT noisy images reconstructed with and without AC for different iterations. Images were reconstructed using OS-EM algorithm with four subsets and no postfiltering was applied. (b) Image noise level as a function of defect contrast for PH and R4SSH SPECT without and with AC for different iterations.

sensitivity for R4SSH SPECT with the same acquisition time in this study. There was no additional CT scan for the R4SSH MPS due to radiation dose concerns.

The R4SSH data were reconstructed with the OS-EM algorithm with five subsets with compensations for attenuation and CDR (Ref. 9) and window-based scatter correction.[22] The PH SPECT data were reconstructed with the Astonish® package (Philips Medical Systems, Milpitas, CA) using the OS-EM algorithm including compensations for attenuation, CDR, and scatter. In both R4SSH and PH SPECT, the same attenuation map converted from the CT image acquired during the PH SPECT stress study was used for attenuation compensation. According to the clinical protocol at Johns Hopkins Outpatient Center, the PH SPECT projections were zoomed with a factor of 1.46 and reconstructed into $64 \times 64 \times 64$ matrices with pixel sizes of 0.64 cm. Without zooming, the R4SSH SPECT projection was reconstructed into $128 \times 128 \times 128$ matrices with pixel sizes of 0.47 cm.

III. RESULTS

III.A. Computer simulations

Figure 3(a) shows the sample noisy short-axis PH and R4SSH SPECT images reconstructed without and with AC. There was no defect in the shown slice and thus the phantom activity was uniform over the whole myocardium. Images are shown without postfiltering. The liver in R4SSH images was truncated due to the limited CVOV. However, the left ventricle was fully within the CVOV. For the images both without and with AC, the R4SSH images have substantially lower noise than those of PH images, particularly for the images with higher iteration numbers. For both PH and R4SSH SPECT, images reconstructed without AC have lower intensity in the inferior region due to the attenuation effect, while images with AC are more uniform around the whole myocardium region.

Figure 3(b) shows the relationship between averaged NSD and defect contrast for PH and R4SSH SPECT without and with AC. The points on the curves represent number of iterations for OS-EM. For each curve, the iteration number increases from left side to the right side. The curves toward the bottom right region correspond to the images with lower noise and higher contrast, indicating superior image quality. Clearly, the curves of R4SSH SPECT are more toward the bottom right region than the curves of PH SPECT, and the R4SSH SPECT with AC has the lowest curve indicating the best noise-contrast trade-off among the four curves.

III.B. CHO and ROC study

In the CHO study, we optimized the number of iterations for OS-EM and cutoff frequency for the Butterworth postfilter in terms of the AUC values for PH and R4SSH SPECT without and with AC. Figure 4(a) shows the AUC values as a function of number of iterations for the optimal cutoff frequencies optimized in Fig. 4(b). Figure 4(b) shows the AUC values as a function of cutoff frequency for the optimal iteration numbers optimized in Fig. 4(a). We evaluated sets of iteration numbers and cutoff frequencies to determine the optimal parameters, and Figs. 4(a) and 4(b) just showed the data with the optimized parameters rather than all the data for clear figure visualization. The results showed that the defect detectability in terms of AUC values is more sensitive to the cutoff frequency than to the iteration number. Figure 4(b) shows that the AUC values for each curve do not have large differences as long as the optimized cutoff frequency is chosen.

The combinations of iteration number and cutoff frequency giving the highest AUC values are considered as the optimal parameters. We compared the best performance of PH and R4SSH SPECT without and with AC in terms of the highest AUC values. As shown in Fig. 4(c) and Table II, statistical tests using the CLABROC program showed that for

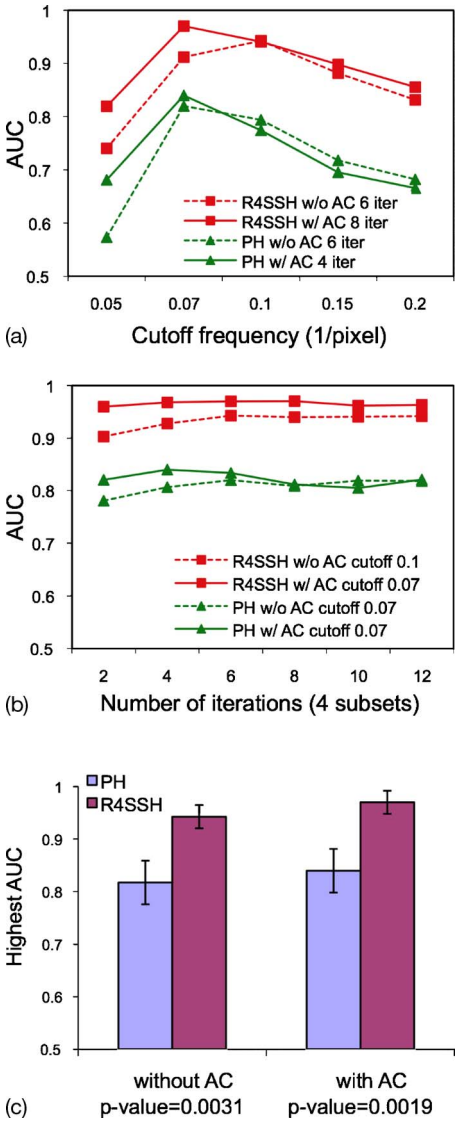

FIG. 4. (a) AUC as a function of cutoff frequencies for R4SSH and PH SPECT with the optimized number of iterations. (b) AUC as a function of number of iterations for R4SSH and PH SPECT with the optimized cutoff frequencies. (c) Highest AUCs with standard deviations for R4SSH and PH SPECT without and with AC.

both without and with AC, R4SSH SPECT has significantly higher defect detectability than that of PH SPECT, with p-values <0.01. For both PH and R4SSH SPECT, AC improves the defect detectability with slightly higher AUC, but the improvement is not statistically significant using the data sets in this study.

III.C. Phantom studies

Figure 5 shows three different slices of short and horizontal long axis images of PH and R4SSH SPECT. With only 7.5 min acquisition, R4SSH SPECT images gave similar noise level and image quality visually as that of PH SPECT images with 21 min acquisition.

III.D. Patient studies

Patient characteristics are shown in Table III. Figure 6 shows the resliced sample reconstruction results of the first patient study. We found that with only one camera, from visual observation, the R4SSH SPECT images showed overall similar noise level and image quality as that of the PH SPECT images.

IV. DISCUSSION

In this paper, we evaluated the performance of R4SSH myocardial perfusion SPECT with respect to conventional SPECT with parallel-hole collimators using computer simulation, ROC analysis, phantom studies, and patient studies. With high sensitivity, the R4SSH SPECT shows a potential to improve the overall myocardial SPECT image quality and patient workflow.

In the computer simulation study with the same acquisition time, the R4SSH SPECT images showed lower noise than the PH SPECT images in terms of both visual observation and noise measurements. This demonstrated the noise benefit of R4SSH SPECT images due to the high sensitivity property.

In the CHO and ROC study, we optimized the number of iterations for OS-EM and cutoff frequencies of Butterworth filter in terms of AUC values and demonstrated that R4SSH SPECT gave improved defect detectability than PH SPECT for the patient (phantom) population and defect detection task in this study. With other phantom population and tasks, we expect the R4SSH SPECT would also yield improved detectability than PH SPECT, but the statistical difference may be varied depending on the object variability included in the study.[23] Therefore, the optimal parameters in the CHO study may not be generalized to other studies, but the results showing the advantage of R4SSH SPECT over PH SPECT can be applied elsewhere. Figures 4(a) and 4(b) showed that

TABLE II. Test for statistical significance between different imaging methods with highest AUC using optimized parameters.

Method 1	Method 2	AUC mean for Method 1	AUC standard deviation for Method 1	AUC mean for Method 2	AUC standard deviation for Method 2	p-value	Statistically significant
PH w/o AC	R4SSH w/o AC	0.817	0.042	0.943	0.022	0.0031	Yes
PH w/AC	R4SSH w/AC	0.839	0.039	0.971	0.014	0.0019	Yes
PH w/o AC	PH w/AC	0.817	0.042	0.839	0.039	0.3460	No
R4SSH w/o AC	R4SSH w/AC	0.943	0.022	0.971	0.014	0.1048	No

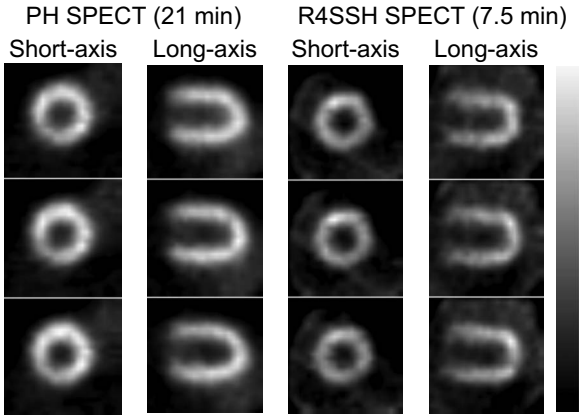

FIG. 5. Sample reconstructed slices of PH and R4SSH SEPCT with different acquisition times in the phantom experiment. No postfiltering was applied.

TABLE III. Patient characteristics.

Patient index	Gender	Weight (lbs)
1	Female	212
2	Male	250
3	Male	157
4	Female	N/A[a]
5	Male	167

[a]The acquisition failed at the beginning, therefore this patient was not included in the data analysis and no weight information can be retrieved.

the defect detectability in terms of the AUC values is more sensitive to the cutoff frequency of the postfilter than to the number of iterations. This may indicate that radiologists should be careful with choosing the cutoff frequencies for more accurate diagnosis.

The R4SSH SPECT images in the phantom study with 1/3 acquisition time and images in the patient studies using only one detector showed similar image quality as those of PH SPECT with two detectors due to the high sensitivity of R4SSH collimator. This indicated that the acquisition time or patient dose can be greatly reduced by using R4SSH SPECT without sacrificing image quality. Nowadays, most modern SPECT are dual-head systems with twice the sensitivity compared to single-head systems with the same acquisition time. To take the full advantage of dual-head systems and further improve the system efficiency, our future plan is to have two RMSSH collimators mounted on both detector heads of a dual-head SPECT system. Since RMSSH SPECT uses three or four camera positions to acquire projection data,[6,7] with the gantry flexibility of the Philips Precedence® system, both detector heads can be tilted and positioned to acquire projection data of two camera positions first, and then moved to the other two camera positions to finish data acquisition. The projection data from all four camera positions acquired by the two detectors will then be sorted to form a complete projection data set that is identical to what is acquired by using a single detector head for reconstruction, without imposing additional degradations such as truncation artifact. With two gamma cameras both equipped with RMSSH collimators that can acquire data simultaneously, the efficiency of the whole system would double compared to that using only one RMSSH collimator.

So far, we have conducted this pilot clinical study for five patients. The first, third, and fifth study showed promising results, while we had problems with acquiring desired data for the second and fourth study. For the second patient study, the patient was too wide to be fitted into the R4SSH acquisition geometry. This resulted in undesirable images where the heart was not at the center of CVOV (Fig. 7). For the fourth patient study, the contrast of the heart on the control screen of the Precedence® system was too low to discriminate heart from the background, thus we could not determine the camera positions based on the centroids of heart projection. For the other three patient studies, the data acquisition went smoothly. It usually took about 15–25 min in total to change the collimator from PH to R4SSH, set up the rotating

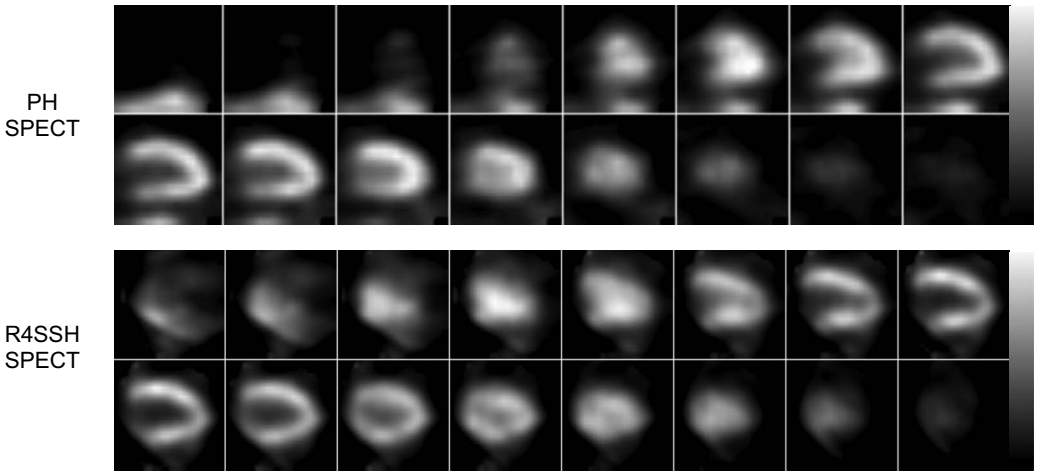

FIG. 6. Sample PH and R4SSH SPECT reconstructed horizontal long axis slices of the first patient study. Both images were reconstructed with the compensations of attenuation, scatter, and collimator-detector response. No postfiltering was applied. PH images are at the fifth iteration with four subsets (20 updates). R4SSH images are at the fourth iteration with five subsets (20 updates).

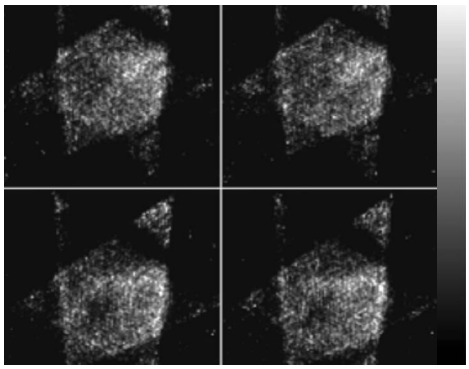

FIG. 7. Sample R4SSH SPECT reconstructed transaxial slices (without post-filtering) of the second patient study, which failed to center the heart in the CVOV due to the patient size.

motor and list-mode acquisition, and determine each camera position. The difficulty of the second patient study may lead to a new collimator design with larger CVOV and longer distance from the center of CVOV to the collimator surface.[24] Incorporating x-ray scout scan into patient positioning in the future may solve the difficulty of the fourth patient study.

To implement the AC in patient study, we used the AC map derived from CT images acquired from PH SPECT study. We did not acquire another CT image during R4SSH SPECT as we do not want to give additional radiation dose to the volunteered patients. Since the patient position for PH and R4SSH SPECT may be slightly different, the R4SSH SPECT images with AC using PH SPECT attenuation map may suffer from misregistration. To solve this in future studies, we can either acquire AC map during the R4SSH SPECT study or implement some rigid/nonrigid transformation to the PH SPECT AC map so that the AC map for the R4SSH SPECT fully aligns with the emission images.

The extra cost for R4SSH SPECT mainly comes from fabricating R4SSH collimators and they can be mounted onto any standard clinical SPECT system that already has a huge installation base. Thus, the current SPECT systems can be easily upgraded to include R4SSH SPECT capability with minimal additional cost.

V. CONCLUSIONS

Due to the high sensitivity property, the RMSSH SPECT has a great potential to improve the CAD detection and workflow of SPECT imaging acquisition. The clinical benefits of RMSSH SPECT need to be further explored through clinical trials.

ACKNOWLEDGMENTS

This work is supported by the National Institutes of Health under Grant No. R01-EB001983. The authors thank Philips Medical System for the technical support of the Precedence® SPECT/CT system and list-mode acquisition. Thanks also go to Eric Frey, Xin He, and Yuchuan Wang for helpful discussions; Si Chen for writing the motor control program; Xiaolan Wang for help with reslicing the cardiac images; Linda Wilkins and Susanne Bonekamp for coordinating patient studies; and Erico Blomer for his help with installing the R4SSH collimator onto the Precedence® system and other scanner-related problems in the studies.

[a]Electronic mail: cliu2@u.washington.edu; Present address: 222 old Fisheries Building, Box 357987, 4000 15th Avenue NE, University of Washington, Seattle, WA 98195.

[1]W. Chang, S. L. Lin, and R. E. Henkin, "A new collimator for cardiac tomography: The quadrant slant-hole collimator," J. Nucl. Med. **23**, 830–835 (1982).
[2]S. M. Dale, D. E. Bone, L. A. Brodin, and C. Lindstrom, "Comparison of SPECT and ectomography for evaluating myocardial perfusion with technetium-99m-sestamibi," J. Nucl. Med. **38**, 754–759 (1997).
[3]G. Bal, R. Clackdoyle, D. J. Kadrmas, G. L. Zeng, and P. E. Christian, "Evaluating rotating slant-hole SPECT with respect to parallel hole SPECT," in the Record of IEEE Nuclear Science Symposium and Medical Imaging Conference, 2000, Vol. 22, pp. 67–71.
[4]G. Bal, E. V. R. DiBella, G. T. Gullberg, and G. L. Zeng, "Cardiac imaging using a four-segment slant-hole collimator," IEEE Trans. Nucl. Sci. **53**, 2619–2627 (2006).
[5]J. Roberts, R. Maddula, R. Clackdoyle, E. DiBella, and Z. Fu, "The effect of acquisition interval and spatial resolution on dynamic cardiac imaging with a stationary SPECT camera," Phys. Med. Biol. **52**, 4525–4540 (2007).
[6]D. E. Wessell, "Rotating slant-hole single photon emission computed tomography," Ph.D. thesis, Department of Biomedical Engineering, The University of North Carolina at Chapel Hill, 1999.
[7]S. S. Orlov, "Theory of 3-dimensional reconstruction. 1. Conditions for a full set of projections," Kristallografiya **20**(3), 511–515 (1975).
[8]W. P. Segars, "Development and application of the new dynamic NURBS-based cardiac torso (NCAT) phantom," Ph.D. thesis, Department of Biomedical Engineering, The University of North Carolina at Chapel Hill, 2001.
[9]J. Xu, C. Liu, Y. Wang, E. C. Frey, and B. M. W. Tsui, "Quantitative rotating multi-segment slant-hole SPECT mammography with attenuation and collimator-detector response compensation," IEEE Trans. Med. Imaging **26**(7), 906–916 (2007).
[10]H. M. Hudson and R. S. Larkin, "Accelerated image-reconstruction using ordered subsets of projection data," IEEE Trans. Med. Imaging **13**(4), 601–609 (1994).
[11]K. J. Myers and H. H. Barrett, "Addition of a channel mechanism to the ideal-observer model," J. Opt. Soc. Am. A **4**(12), 2447–2457 (1987).
[12]H. H. Barrett, J. Yao, J. P. Rolland, and K. J. Myers, "Model observers for assessment of image quality," Proc. Natl. Acad. Sci. U.S.A. **90**(21), 9758–9765 (1993).
[13]X. He, E. Frey, J. Links, K. Gilland, W. Segars, and B. Tsui, "A mathematical observer study for the evaluation and optimization of compensation methods for myocardial SPECT using a phantom population that realistically models patient variability," IEEE Trans. Nucl. Sci. **51**(1), 218–224 (2004).
[14]E. Frey, K. Gilland, and B. Tsui, "Application of task-based measures of image quality to optimization and evaluation of three-dimensional reconstruction-based compensation methods in myocardial perfusion SPECT," IEEE Trans. Med. Imaging **21**(9), 1040–1050 (2002).
[15]S. D. Wollenweber, B. M. W. Tsui, E. C. Frey, D. S. Lalush, and K. J. LaCroix, "Comparison of human and channelized Hotelling observers in myocardial defect detection in SPECT," J. Nucl. Med. **39**(5), 170–170 (1998).
[16]S. D. Wollenweber, B. M. W. Tsui, D. S. Lalush, E. C. Frey, and G. T. Gullberg, "Evaluation of myocardial defect detection between parallel-hole and fan-beam SPECT using the Hotelling trace," IEEE Trans. Nucl. Sci. **45**(4), 2205–2210 (1998).
[17]C. E. Metz, "Basic principles of ROC analysis," Semin Nucl. Med. **8**(4), 283–298 (1978).
[18]C. E. Metz, "Some practical issues of experimental-design and data-analysis in radiological ROC studies," Invest. Radiol. **24**(3), 234–245 (1989).
[19]C. E. Metz, "ROC methodology in radiologic imaging," Invest. Radiol. **21**(9), 720–733 (1986).
[20]C. E. Metz, in *Multiple Regression Analysis: Applications in the Health*

Sciences, edited by D. Herbert and R. Myers (American Institute of Physics, New York, 1986), pp. 365–384.
[21]C. E. Metz, B. A. Herman, and J. H. Shen, "Maximum likelihood estimation of receiver operating characteristic (ROC) curves from continuously-distributed data," Stat. Med. **17**(9), 1033–1053 (1998).
[22]M. F. Smith and R. J. Jaszczak, "Generalized dual-energy-window scatter compensation in spatially varying media for SPECT," Phys. Med. Biol. **39**, 531–546 (1994).
[23]C. Liu, J. Xu, and B. M. W. Tsui, "The effects of object variability on the channelized hotelling observer performance in the evaluation of R4SSH and PH myocardial perfusion SPECT," in the Record of IEEE Nuclear Science Symposium and Medical Imaging Conference, 2006, pp. 1995–1999.
[24]C. Liu, J. Xu, and B. M. W. Tsui, "Development and evaluation of rotating multi-segment variable-angle slant-hole SPECT," J. Nucl. Med. **48**(2), 161–162 (2007).